# A Tuned Microwave Resonant Sensor for Skin Cancerous Tumor Diagnosis

Sen Bing<sup>®</sup>, *Graduate Student Member, IEEE*, Khengdauliu Chawang<sup>®</sup>, *Student Member, IEEE*, and J.-C. Chiao<sup>®</sup>, *Fellow, IEEE* 

Abstract—In this work, a planar microwave sensor based on a flexible polyimide substrate has been developed to distinguish if a skin lesion is malignant or benign. The sensor is a tuned loop resonator operating in the industrial, scientific, and medical (ISM) band at 2.465 GHz, providing a localized high-intensity electric field that penetrates into tissues with sufficient spatial and spectral resolutions. The loop resonator with a radius of 5.4 mm was tuned by a concentric metal pad to the desired resonant frequency with a sufficiently high quality factor of 98.7 and a reflection coefficient of -63.98 dB. The sensor is based on the detection of electromagnetic resonance change and sequential frequency shift that is susceptible to the dielectric property difference between cancerous and benign tissues. Basal Cell Carcinoma (BCC) and Seborrheic Keratosis (SK), the most commonly found malignant and benign skin lesions with close visual similarities, were selected to demonstrate the sensing concept. Tissue-mimicking materials were fabricated to have similar dielectric properties to those of healthy skin, SK, and BCC tissues in the literature. Simulations and measurements were conducted. Significant frequency shifts of 759 MHz and 415 MHz were observed between BCC and SK phantoms in simulations and measurements, respectively, when the size of the tumor phantom was a cuboid of 12 mm imes 12 mm imes 4 mm underneath and among healthy skin. Simulations were conducted for different cuboid side lengths from 2 to 16 mm while the thickness remained at 4 mm. Malignant lesions could be distinguished with a cuboid side length as small as 2 mm. Corresponding measurements for cuboid side lengths of 6, 8, 10, and 12 mm were conducted and matched the trend well with the simulation results. The promising results in simulations and measurements validate the sensing principle, showing great potential for skin cancer detection in a noninvasive, efficient, and lower-cost way.

Index Terms—Basal cell carcinoma (BCC), loop resonator, nondestructive evaluation (NDE), skin cancer, tuned.

#### I. INTRODUCTION

KIN cancer screening is urgently needed in regular clinical diagnosis due to its high occurrence and large populations of patients [1]. The Skin Cancer Foundation estimates that over 187,000 new cases of skin cancers will be diagnosed in the US in 2023 [2]. Skin cancers are roughly categorized into three cell types: basal cells, squamous cells, and melanoma cells [3]. The

Manuscript received 17 April 2023; revised 19 May 2023; accepted 25 May 2023. This work was supported in part by the National Science Foundation under Grant ENG-CMMI-1929953, and in part by the Mary and Richard Templeton endowment. (Corresponding author: Sen Bing.)

The authors are with the Department of Electrical and Computer Engineering, Southern Methodist University, Dallas, TX 75205 USA (e-mail: sbing@smu.edu; kchawang@smu.edu; jchiao@smu.edu).

Digital Object Identifier 10.1109/JERM.2023.3281726

first two types can be grouped into non-melanoma skin cancers, and most skin cancer occurrences are the non-melanoma type [4]. The lesion area usually can be seen by the naked eye as its color and shape change over time, but it is required to be further investigated if the lesion part is cancerous or benign. For example, even experienced caregivers often confuse the Seborrheic Keratosis (non-cancerous) as a Basal Cell Carcinoma lesion, which may lead to unnecessary biopsies due to suspicion of malignancy [5]. Dermoscopy based on visual analysis is typically the primary skin cancer diagnosis [4], [6]. However, its resolution is limited [3], [7], [8], [9] and accuracy has been highly variable since it mainly depends on the examiner's skill and experience [9], [10], which may increase false positives or unnecessary biopsies. The unnecessary intervention can exaggerate further dermal complications such as scarring, bruising, and infection, especially on the faces, and increase patients' stress and financial burdens [11]. The biopsy procedure is an invasive process that can cause pain, anxiety, and disfigurement in patients. The histopathological procedures can take several days to produce results. Typically, around 15–30 benign lesions must be biopsied to diagnose a single case of cancer [12]. Additionally, due to tissue processing and sectioning, a maximum of only 2% samples sent for pathology examination are actually analyzed [13]. Such high costs and inconvenience add behavioral delay [14] for regular check-ups in the potential cancer patient populations, which reduces early or pre-stage cancer identification. The possibility of metastasis and cancer cell migration increases significantly once the skin tissue becomes malignant. Metastasis reduces the survival rate of patients dramatically and can be avoided with a timely diagnosis and treatment [15], [16]. Thus, a more convenient, accurate, and noninvasive method with lower costs suitable for large-population skin cancer screening is needed.

Noninvasive methods, such as bioimpedance measurements, thermography, and ultrasound, suffer from low accuracy and higher costs [17], [18], [19], [20], [21], [22], [23], [24]. Nonionizing electromagnetic waves may provide a noninvasive evaluation of biological tissues due to the inherently high contrast of dielectric properties among cancerous, benign, and healthy tissues [25], [26], [27], [28], [29], [30]. It has been shown that cancer tumors have distinct water content [26], [31] and biochemistry [32], such as metal concentrations [33], consequently causing significant changes in dielectric properties. With optics, Raman spectroscopy has been used [29] to investigate water content and structural alterations in skin malignancy, specifically

2469-7249 © 2023 IEEE. Personal use is permitted, but republication/redistribution requires IEEE permission. See https://www.ieee.org/publications/rights/index.html for more information.

Basal Cell Carcinoma (BCC). The study revealed an increase of approximately 15% in the free (bulk) water content in malignant BCC tissues compared to normal skin tissues. Millimeter waves (30–300 GHz) have been recently utilized for assessing skin lesions and detecting tumors [34], [35], [36], [37]. Shorter wavelengths provide a higher spatial resolution, however, at the cost of a reduced penetration depth ranging from 600 µm to 1.2 mm [38]. Imaging deeper tissues may become an issue with limited radiation powers. Nevertheless, they have been demonstrated as effective in sensing pathological changes in surface layers or outer tissue layers of excised organs. Working with millimeter waves currently may still require expensive and bulky instruments.

#### II. SENSOR DESIGN AND SIMULATIONS

Microwaves with deeper penetration depths can potentially be used for cancer screening. The interactions of electromagnetic waves with different tissues affect wave scattering. Tissue types can be distinguished by evaluating resonant frequency shifts and magnitude changes in reflection coefficients. Microwave reflectometry system has been used for detecting skin abnormalities. An open-end coaxial probe was used to explore the detection of benign lesions compared to adjacent and distanced normal skins [36]. This technique is similar to the dielectric property probe (N1501 A, Keysight) and compared the magnitudes and phases of reflection coefficients at 0.3–3 GHz. A coplanar waveguide probe performed raster scans to obtain near-field images of fat masses with a fixed standoff distance of  $\lambda/10$  at 14.36 GHz [39]. Fat masses with a size larger than 5 mm can be imaged with more than 20 dB contrast in reflections at a single frequency of 14.36 GHz. The probe could produce high-resolution images and was used to detect malignant tumors from healthy skins and benign lesions with 15 and 8 dB contrasts [40], respectively. Designed for skin measurements, a truncated open-ended coaxial probe was used to sense moles and benign and malignant tumors in multiple subjects with a reflectometry-based system [41]. The magnitudes of reflection coefficients of suspected tumors and healthy skins were compared at 0.25–3 GHz. The complex permittivities of skin, mole, and benign and malignant tumors could be extracted from the magnitude differences across the frequency of interest. The extracted dielectric data show distinguishable profiles and values between four different types of tissues. The results helped us to design our resonator. These promising techniques require the rigid probe to be placed on the skin either at a precisely fixed distance or with consistent pressure, which can be difficult as human skins are elastic. Thus, we focus our effort on a conformable solution.

Compared to sophisticated instruments, microwave resonators usually have a compact size. Circuits, antennas, or resonators fabricated on monolithic, flexible substrates can be potentially made into a wearable conforming to the skin. However, most planar resonators fail to provide sufficiently high-intensity fields and spatial resolutions into the tissues due to their poor resonance at microwaves, suffering from low sensitivity. Additional dynamic matching circuits may achieve a high-quality factor, but they are bulky with design constraints, increase insertion

losses and limit resonance frequency ranges. It is challenging to tune the impedance and achieve a high-quality factor in such a conformal microwave resonator without losing the advantages of being small and planar. Our preliminary work [42] has developed a simple self-tuned method for impedance-matching of planar-loop resonators by embedding a center metal pad. The presence of the metal pad provides distributed capacitance [43] and mutual inductance [44], variable with the gap spacing between the loop and pad, matching the port impedance at the desired operating frequency. Without changing the overall loop size or adding additional tuning circuits outside of the loop, the resonance of the planar loop is improved significantly. Furthermore, the tuned loop can be made of thin-film metal on a polymeric substrate while maintaining a compact size with high resonance performance, providing great potential for near-field sensing on curved surfaces. Applications based on the tuned loop structures have been investigated for wireless power transfer, subcutaneous implant localization [45], [46], human hydration monitoring [47], [48], and breast cancer imaging [49]. This work aims to utilize a similar device architecture as a noninvasive sensor to screen skin lesion types.

Lesion areas could often be ambiguous due to the visual similarity between malignant and benign tissues [5], [50], [51]. Basal Cell Carcinoma (BCC) is the most common malignant tumor cells of the skin, while Seborrheic Keratosis (SK) is one of the most common benign skin tumors [52]. They have close visual similarities as representative pigmented skin tumors [53], [54], which make it difficult to distinguish clinically by eyes. However, they have high contrast in dielectric properties. Thus, BCC and SK cell properties are selected to demonstrate the feasibility of determining whether the lesion area is malignant or benign by our sensor. According to the literature, cancerous BCC has significantly higher dielectric properties than those of healthy skin or benign lesions [28]. Fig. 1 shows the dielectric properties of BCC, SK, and healthy skin obtained from the fourth-order Cole-Cole model by in-vivo measurements [4]. Our initial resonator design and simulations are based on the dielectric properties data in Fig. 1.

Considering the curvatures of the body parts, the tuned loop is designed on a flexible polyimide film (DuPont Pyralux FR9220R) that can have firm contact with the skin. The thickness of the film is 76 µm with a dielectric constant of 3.2, and the copper thickness is 70 µm. The substrate parameters in simulations are the same as the ones in fabrication. Fig. 2 shows the configuration of the tuned loop with a photo of the sensor. The sensor is designed to operate in an ISM (Industrial, Scientific, and Medical) band at 2.465 GHz with considerations for a compact size and sufficient field depths. The loop radius is b = 5.4 mm with a connecting stub length L = 1.5 mm. The metal width w is 0.8 mm. The gap between the loop and the center pad is d = 1.13 mm, which tunes and optimizes the resonance up to -63.98 dB with a quality factor of 98.7 when it is placed on the skin. Fig. 3 shows the simulation setup. The simulation phantom consists of healthy skin and lesion tissue parts. The lesion tissue is set as a 12 mm  $\times$  12 mm  $\times$  4 mm cuboid surrounded by healthy skin. The sensor is directly above the lesion on the skin. The robust resonance provides confined

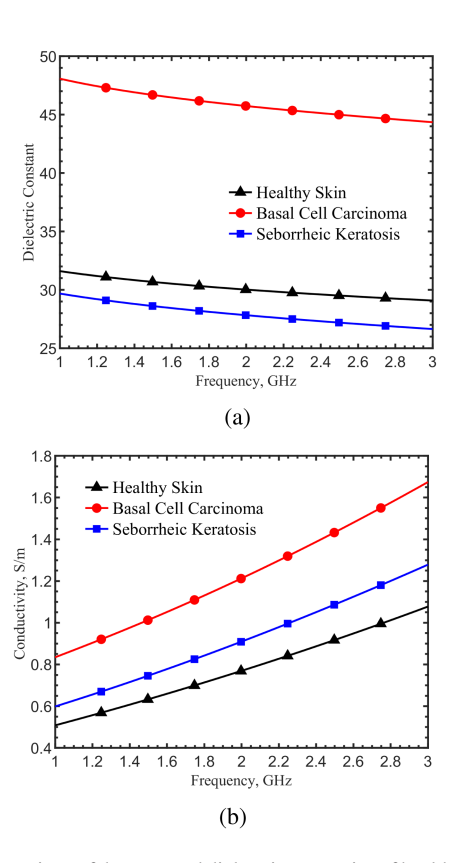


Fig. 1. Comparison of documented dielectric properties of healthy skin, Basal Cell Carcinoma (BCC), and Seborrheic Keratosis (SK) tissues. (a) Dielectric constant and (b) conductivity.

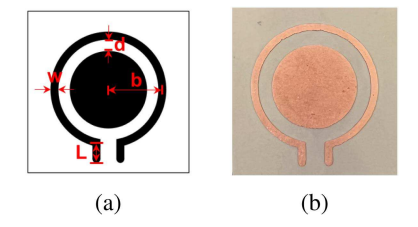


Fig. 2. (a) Configuration of the tuned sensor with radius b=5.4 mm, loop width w=0.8 mm, stub length L=1.5 mm, and tuning gap d=1.13 mm. (b) Photograph of the tuned sensor on a flexible polyimide substrate in its flat condition.

electric field distributions into the skin tissues, as shown in Fig. 4. Fig. 4(a) shows strong fields across the gap and around the loop. The -10-dB and -20-dB attenuation depths from the surface of the loop, in Fig. 4(b), are 10 mm and 18 mm, respectively, providing confined fields deep enough to penetrate through the epidermis layer and detect abnormality up to the dermis and hypodermis layers. As a result, the resonator provides a higher sensitivity to detect effective permittivities contributed by skin tissues while limiting its probing to a spatially confined area.

Finite-element simulations were conducted with the configuration in Fig. 3 and phantoms, including Seborrheic Keratosis (SK), Basal Cell Carcinoma (BCC), and healthy skin tissues. Fig. 5 shows the simulation results of reflection coefficients. The resonance is optimized for the healthy skin condition at

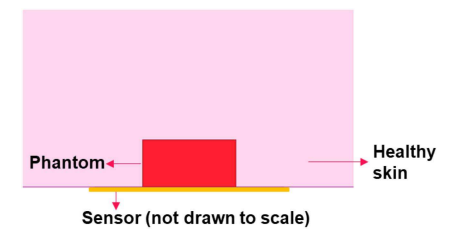


Fig. 3. Schematic simulation setup for the sensor designed to differentiate benign and cancerous phantoms embedded in the healthy skin.

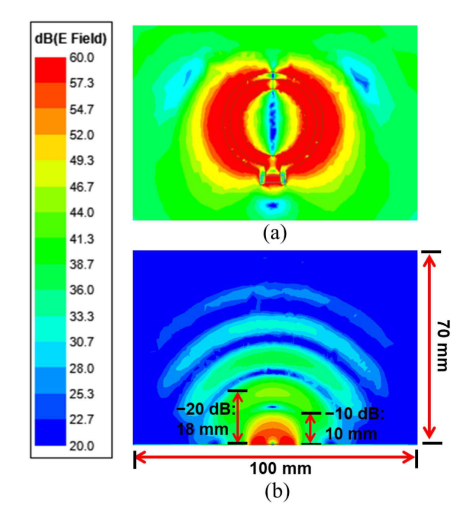


Fig. 4. Cross sections of electric field distributions of the tuned loop resonator: (a) Top view, and (b) side view.

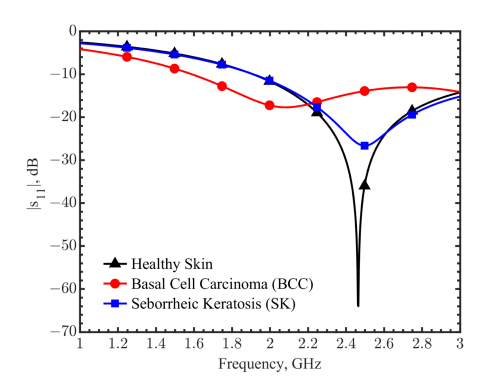


Fig. 5. Comparison of reflection coefficients for healthy skin, Basal Cell Carcinoma (BCC), and Seborrheic Keratosis (SK) tissues at frequencies band 1–3 GHz.

2.465 GHz with  $|s_{11}|$  of -63.98 dB. BCC has a resonant frequency of 2.08 GHz with  $|s_{11}|$  of -17.68 dB, whereas SK has a resonant frequency at 2.5 GHz with  $|s_{11}|$  of -26.62 dB. The frequency shift between SK (benign) and BCC (cancerous) is 0.42 GHz. The frequency shift is 0.39 GHz from the healthy skin to BCC. The frequency shifts are distinguishable.

To further test the performance, more simulations were conducted for different tumors with side lengths of the cuboid phantoms from 2 to 16 mm. The phantom thickness was kept at

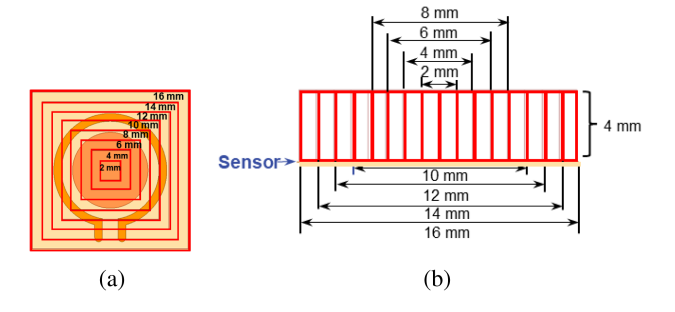


Fig. 6. Comparison of tumor sizes and sensor dimensions. (a) Top view and (b) side view. The tumor's square side lengths range from 4 to 16 mm with a constant thickness of 4 mm.

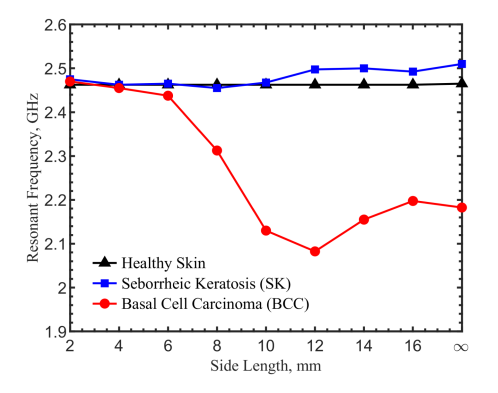


Fig. 7. Resonant frequencies in simulations for healthy skin, and tumors of Basal Cell Carcinoma (BCC) and Seborrheic Keratosis (SK) embedded in the healthy skin. The tumors have a thickness of 4 mm and square side lengths from 2–16 mm, illustrated in Fig. 6. Complete phantoms made of BCC and SK materials have side lengths of infinite.

4 mm. The size comparison between the tumor and sensor is illustrated in Fig. 6, where the red lines indicate tumor boundaries. Reflection coefficients are collected for each configuration, and resonant frequencies are compared in Fig. 7. When the cuboid tumor side length exceeds 6 mm, a noticeable difference in resonant frequency shifts is observed between BCC and SK. When the tumors are equal to or smaller than 6 mm on the side, they are located in the areas where the electric fields are weak, based on Fig. 4. As a result, the resonant frequency shifts are limited in these cases. However, by utilizing oversampling in spatial scans to place the lesion area under the strong fields, small tumors with a side length of as small as 2 mm can be detected. Further details regarding the use of oversampling to improve the detection of smaller tumors will be discussed later.

### III. MEASUREMENTS

# A. Artificial Tumor Phantoms

As this study mainly concerns concept validation, tissue-mimicking materials (TMMs) were created to imitate simulated tissue types, including Basal Cell Carcinoma (BCC), Seborrheic Keratosis (SK), and healthy skin. This is because of practical and clinical challenges to produce controlled and sufficiently large tissue samples from biopsies. The samples may also become dehydrated after being removed from the skin. It is also a great

challenge to perform in-vivo measurements directly on patients at this feasibility study period due to the limited availability of patients with controlled tumor types. Therefore, we decided to create artificial tumor phantoms with dielectric properties documented in the literature. Amir et al. [55] developed semisolid phantoms to simulate human skin and skin tumors by altering the mixtures of conductive filler and polymer matrix. Likewise, Garrett et al. [56] presented dielectric tunable tissue-mimicking materials (TMMs) composed of urethane rubber, graphite powders, and carbon black powders. Both approaches produced stable, ultrawideband, and tunable skin-equivalent phantoms.

Following the methodology by Garrett et al. [56], PMC-121 urethane rubber (Smooth-On Inc, Texas) was chosen as the polymer matrix with conductive fillers consisting of graphite powders (Sigma-Aldrich, Saint Louis) and carbon black powders (Thermo Fisher Scientific, Massachusetts) incorporated. By varying the concentrations of the conductive fillers, the dielectric properties of the TMMs were adjusted. Phantoms with healthy skin, BCC, SK tissues were made in a cylindrical shape with a diameter of 10 cm and a thickness of 3 cm. Dielectric properties were measured using a broadband, open-ended coaxial probe kit (Keysight N1501 A) [57]. The flange-free probe provided firm contact with the material. Four measurements were taken in four different locations at least 5 cm apart to avoid overlapping volumes [36]. The averages were calculated from four measurements for each phantom. After adjusting the conductive filler concentrations, three TMMs were finalized with different combinations of graphite and carbon black powders, corresponding to healthy skin (17.9%-wt & 12.1%-wt), BCC (25.6%-wt & 11.9%-wt), and SK (5.6%-wt & 12.1%-wt). The measured dielectric properties of these three phantoms were plotted in Fig. 8, and error bars were derived from four measurements taken for each phantom. It should be noted that the error bars might be due to the contact pressures from the probe to the phantoms and imperfect/nonuniform mixtures of powders in polymer matrices. When the powder concentrations increased, the mixtures hardened, making it difficult to mix uniformly.

Similar to the simulations, the dielectric properties of cancerous and benign tissues exhibited high contrasts. However, discrepancies in the dielectric properties across the frequencies between the fabricated TMMs and simulation phantoms were expected because the spectral profiles of the dielectric properties in the polymer matrix did not follow exactly those of tissues documented in the literature. It should also be noticed that the dielectric properties data from a Cole-Cole model [4] were derived from averages among multiple measurements with clear deviations in the data. With these observations, the measured dielectric property data in the final phantom design were within the range of the in-vivo skin cancer measurements in [4].

## B. Results

The fabricated BCC and SK phantoms were sliced into small pieces with dimensions of 12 mm  $\times$  12 mm  $\times$  4  $\times$  mm and inserted into the healthy skin phantom. The measurement setup and photo are shown in Fig. 9. To ensure a stable and firm contact, a medical-grade tape (3 M Nexcare Durapore Durable

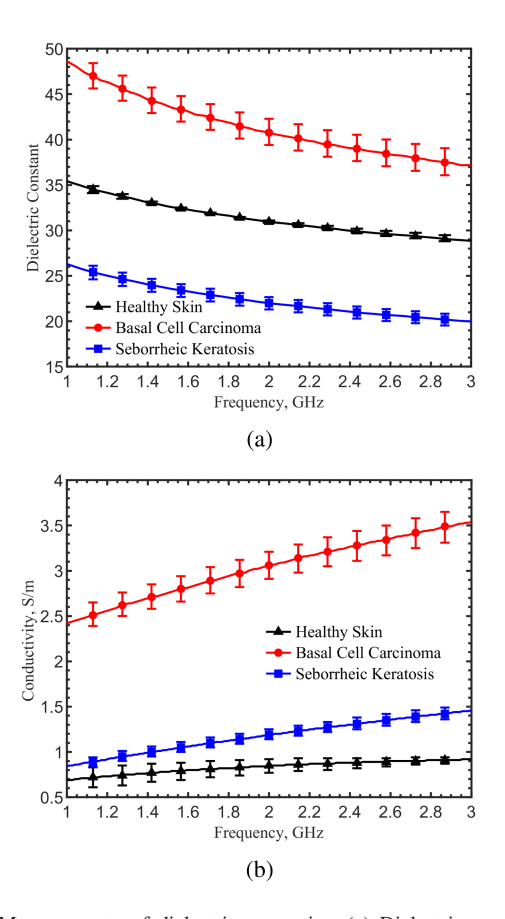


Fig. 8. Measurements of dielectric properties: (a) Dielectric constant and (b) conductivity in the phantoms made of tissue-mimicking materials. The dielectric properties mimic the healthy skin, Basal Cell Carcinoma (BCC), and Seborrheic Keratosis (SK) tissues. The error bars were obtained from 4 measurements with respect to their averaged values.

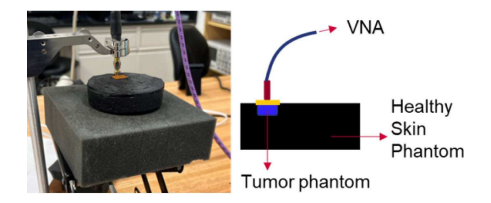


Fig. 9. Setup of skin cancer measurements using custom-made tissuemimicking materials.

Cloth Tape, USA) was used to attach the sensor to the phantom. The sensor was connected to a vector network analyzer (Keysight PNA N5227B). Measurements were conducted with the BCC and SK inside the healthy skin phantoms and a single healthy skin phantom. The resonant frequency of the BCC-inskin phantom was 1.6 GHz and shifted to 2.36 GHz for the SK-in-skin phantom, as shown in Fig. 10. The healthy skin phantom had a resonant frequency of 2.2 GHz. The spectral shapes in three different scenarios matched with simulations. Discrepancies existed between simulations and measurements, primarily were due to the difference in the dielectric properties from the literature used in the simulations and those measured in the phantoms. The frequency shift between BCC and healthy

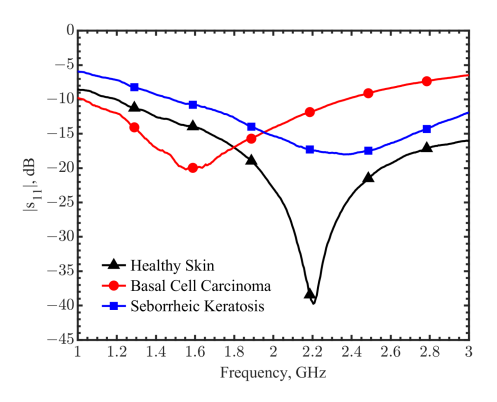


Fig. 10. Reflection coefficients in measurements for healthy skin phantom, Basal Cell Carcinoma (BCC), and Seborrheic Keratosis (SK) tumor phantoms embedded in healthy skin at the frequency band of 1–3 GHz.

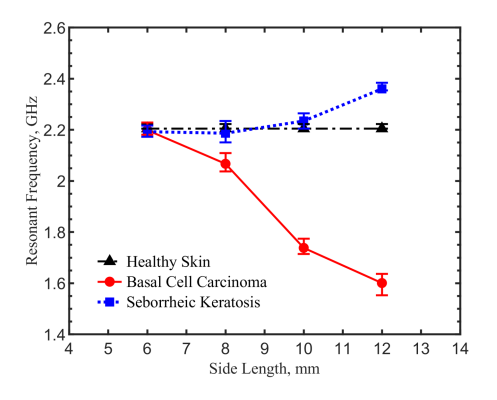


Fig. 11. Measured resonant frequencies for healthy skin, and Basal Cell Carcinoma (BCC) and Seborrheic Keratosis (SK) tumors in the skin. Tumors have square side lengths of 6, 8, 10, and 12 mm with a thickness of 4 mm.

tissue was  $0.76~\mathrm{GHz}$  (32.18 %) in the measurement, compared to  $0.42~\mathrm{GHz}$  (16.62 %) in the simulations. However, the permittivity and conductivity contrast in the tissues can still be used to recognize tissue types with the resonator.

Similar measurements were conducted for phantoms of  $6 \times 6$ ,  $8 \times 8$ , and  $10 \times 10 \text{ mm}^2$ , all with a thickness of 4 mm. Resonant frequencies for different sizes of tumors are shown in Fig. 11. The error bars were obtained from 5 measurements for each case. The frequency shifts between BCC and SK were 5.9, 119.6, 496.3, and 759.46 MHz for side lengths of 6, 8, 10, and 12 mm, respectively, while the ones in simulations were 27.5, 142.5, 337.5, and 415 MHz, shown in Fig. 7. The distinguishable frequency shifts between BCC and SK in simulations and measurements, demonstrated the feasibility of identifying cancerous and benign tissues using the tuned resonator. In measurements, the size limit of  $6 \times 6 \text{ mm}^2$  matched with simulation results.

# C. Oversampling to Identify Smaller Tumors

During the mentioned tests, the center of the tumor-in-skin phantom was placed directly under the center point of the sensor. The tumor size changed in different measurements, but the centers were aligned. The procedure was to place the resonator loop on the spot where darker colors indicate a potential lesion area in

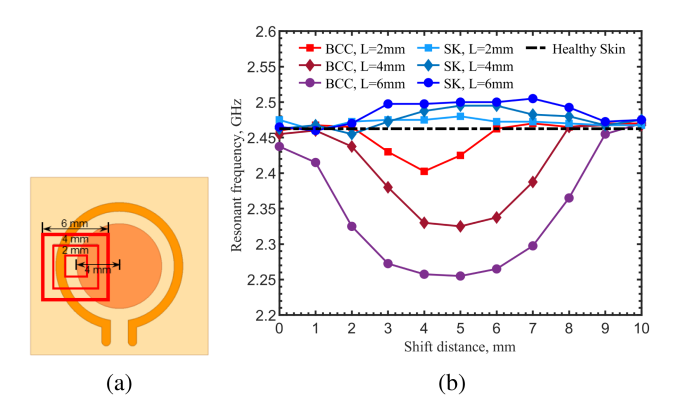


Fig. 12. (a) Setup for oversampling experiment. The sensor is horizontally shifted by 10 mm with a step size of 1 mm. The red squares indicate the lesion volumes of  $2 \times 2 \times 4$ ,  $4 \times 4 \times 4$ , and  $6 \times 6 \times 4$  mm<sup>3</sup> after the tumors move 4 mm from the center. (b) Resonant frequencies for BCC and SK tumors and healthy skin as a function of shifted distance in the oversampling setup.

order to identify the risk of the spot being malignant. Currently, caregivers visually inspect brownish spots or speckles, changing moles, or skin areas with colors changed and irregular borders. Because the spot is visibly defined, after placing the sensor center-to-center on the area of interest, the sensor can be moved off-center spatially to scan the area for oversampling the area. The purpose is to create high confidence before the biopsy is applied. This is particularly important for the skin areas around the eyes, lips, and noses on the faces where it is painful for biopsy or impacts self-perception of the patient's appearance.

When the sensor was placed center-to-center on the spot, it can distinguish tissue types when the tumor was bigger than 6 mm, as shown in Fig. 7. This was due to that the tumor was located within an area where electric fields were weak according to Fig. 4. The effective permittivity change that decided resonance had little contribution by the tumor. Since the high fields were around the ring gap, moving the loop in small steps to oversample the area may provide a better resolution to distinguish the boundary from the high permittivity contrast.

The sensor was moved by 10 mm with a step size of 1 mm orthogonally to its port direction. Fig. 12(a) shows the setup for oversampling as the loop moved horizontally to the left on the skin through the tumor area. The simulations were repeated for lesion sizes of  $2 \times 2$ ,  $4 \times 4$ , and  $6 \times 6$  mm<sup>2</sup>, each has a thickness of 4 mm. The center metal pad had a radius of 4 mm, so when the lesion area shifted a distance of 4 mm to the right, the center of the lesion was directly under the ring gap where the field magnitudes were highest. Resonant frequencies by oversampling are shown in Fig. 12(b). When the distance was zero, the lesion center was directly under the center of the metal pad, so there was no resonant frequency shift for all three sizes of tumors. The resonant frequency shifts were distinguishable between the malignant (BCC) and benign (SK) tumors as 72.5 MHz, 157.5 MHz, and 240 MHz for the lesion side lengths of 2, 4, and 6 mm, respectively. The BCC could be clearly identified from the healthy skin too. Thus, malignant tissues can still be detected in lesions as small as  $2 \times 2 \times 4 \text{ mm}^3$ by the oversampling technique.

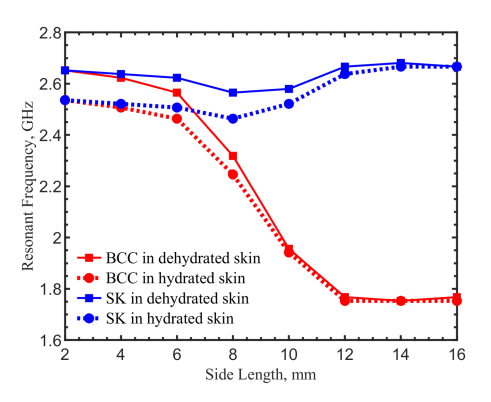


Fig. 13. Comparisons of resonant frequencies between BCC (malignant) and SK (benign) tumors in simulations. The simulation parameters include measured dielectric properties of human skins: fully-hydrated (dashed line) and partially-dehydrated (solid line). The tumors have volumes of  $2 \times 2$  (a side length of 2 mm) to  $16 \times 16$  (a side length of 16 mm) mm<sup>2</sup> with a thickness of 4 mm.

#### D. Sensor Performance in Varied Skin Hydration Conditions

The resonator detects effective permittivity changes due to the differences in dielectric properties in malignant and benign tissues. Skin conditions, such as its water content in the dermis and hypodermis layers due to body hydration levels, may affect sensing results. Documented data [26], [58] shows that the dielectric property difference between dry skin and wet skin is noticeable. Dielectric measurements on the skin of the same person at hydrated and dehydrated status showed the water content factor. And resonant frequency shifts in the resonator were due to the dielectric changes [47], [48]. To investigate the effect from water content variations in the skin, simulations were conducted for tumor cuboids with side lengths from 2 to 16 mm and a thickness of 4 mm, as the same as the ones in Fig. 7. Measured permittivities and conductivities were obtained from human forearms in fully-hydrated and partially-dehydrated statuses. The tumor phantoms were placed in these two different skin conditions. Fig. 13 shows the comparison of resonant frequencies between BCC and SK. Solid curves indicate the resonant frequencies detected on dehydrated skins and dashed ones are for hydrated skins. When the side length is less than 6 mm, there was no frequency shift between BCC and SK in hydrated or dehydrated skin conditions, similar trends as the results in Fig. 7. The frequency shifts above a 6-mm side length were noticeable between BCC and SK lesions considering the area being measured was either hydrated or partially-dehydrated. When the side length is larger than 10 mm, the dielectric properties were dominated by the lesion as the water content effect was decreased. The frequency shifts between BCC and SK for tumor sizes of  $6 \times 6 \times 4 - 16 \times 16 \times 4 \text{ mm}^3$  were 43.5 and 913.5 MHz for a fully hydrated skin condition, while they were 58 and 899 MHz for the partially-dehydrated skin condition, respectively. The sensor was able to distinguish malignant from benign lesions among different hydration levels in the body.

#### IV. CONCLUSION

In this work, we developed a flexible tuned microwave resonator that can conform to the skin to noninvasively identify if the lesion area of interest is cancerous, such as Basal Cell Carcinoma (BCC), or benign, such as Seborrheic Keratosis (SK). It can provide a quick and painless means to assist caregivers to evaluate potential cancerous lesion areas. Simulations and measurements by phantoms were designed to validate the concept feasibility of utilizing a planar tuned loop resonator for noninvasive skin cancer screening. Tissue-mimicking materials with similar documented dielectric properties in the literature of healthy skin, BCC, and SK tissues were used to fabricate phantoms for measurements. The presence of malignant lesions forms a high contrast of permittivities between cancerous and benign tissues. Owing to the robust and high quality factor resonance and sufficient field penetration into the dermis and hypodermis layers of the skin, the tuned loop was able to provide sufficient spatial and spectral resolutions to distinguish malignant lesions as small as  $2 \times 2 \times 4$  mm<sup>3</sup>. Discrepancies between simulations and measurements existed because the documented data in the literature were averaged values, and the materials for making phantoms did not have the same spectral profiles for the skin and tumors. Investigation on the effects caused by skin hydration statuses was conducted by using measured data from fully-hydrated and partially-dehydrated human skins with the tumor phantoms. The distinguishable and consistent trends in different skin conditions showed robust performance by the tuned loop resonator. This work mainly focused on validating the feasibility of a noninvasive skin cancer screening tool with a tuned loop sensor. Phantoms were created because it is difficult to obtain controlled cancerous or benign tissue samples from biopsies. Therefore, future works need to focus on how to create quantifiable and uniform cancerous and benign tumor samples in a repeatable fashion and strategies toward clinical in vivo measurements in patients.

## REFERENCES

- [1] R. L. Siegel, K. D. Miller, H. E. Fuchs, and A. Jemal, "Cancer statistics, 2022." *CA: Cancer J. Clinicians*. vol. 72, no. 1, pp. 7–33, Jan. 2022.
- 2022," CA: Cancer J. Clinicians, vol. 72, no. 1, pp. 7–33, Jan. 2022.
  [2] "Cancer facts & figures 2023," American Cancer Society, Atlanta, GA, USA, 2023. [Online]. Available: https://www.cancer.org/research/cancer-facts-statistics/all-cancer-facts-figures/2023-cancer-facts-figures.html
- [3] V. Narayanamurthy et al., "Skin cancer detection using non-invasive techniques," RSC Adv., vol. 8, no. 49, pp. 2895–2813, Aug. 2018.
- [4] S. A. R. Naqvi, A. T. Mobashsher, B. Mohammed, D. Foong, and A. Abbosh, "Benign and malignant skin lesions: Dielectric characterization, modelling and analysis in frequency band 1 to 14 GHz," *IEEE Trans. Biomed. Eng.*, vol. 70, no. 2, pp. 628–639, Feb. 2023.
- [5] J. I. V. D. Rhee, W. Bergman, and N. A. Kukutsch, "The impact of dermoscopy on the management of pigmented lesions in everyday clinical practice of general dermatologists: A prospective study," *Brit. J. Dermatol.*, vol. 162, no. 3, pp. 563–567, Mar. 2010.
  [6] V. Papageorgiou et al., "The limitations of dermoscopy: False-positive and
- [6] V. Papageorgiou et al., "The limitations of dermoscopy: False-positive and false-negative tumours," J. Eur. Acad. Dermatol. Venereol., vol. 32, no. 6, pp. 879–888, Jun. 2018.
- [7] W. Stolz, R. Schiffner, and W. H. C. Burgdorf, "Dermatoscopy for facial pigmented skin lesions," *Clin. Dermatol.*, vol. 20, no. 3, pp. 276–278, 2002
- [8] R. P. Braun, H. S. Rabinovitz, M. Oliviero, A. W. Kopf, and J.-H. Saurat, "Dermoscopy of pigmented skin lesions," *J. Amer. Acad. Dermatol.*, vol. 52, no. 1, pp. 109–121, 2005.
- [9] C. Rosendahl, P. Tschandl, A. Cameron, and H. Kittler, "Diagnostic accuracy of dermatoscopy for melanocytic and nonmelanocytic pigmented lesions," *J. Amer. Acad. Dermatol.*, vol. 64, no. 6, pp. 1068–1073, Jun. 2011.
- [10] M.-L. Bafounta, A. Beauchet, P. Aegerter, and P. Saiag, "Is dermoscopy (epiluminescence microscopy) useful for the diagnosis of melanoma?: Results of a meta-analysis using techniques adapted to the evaluation of diagnostic tests," *Arch. Dermatol.*, vol. 137, no. 10, pp. 1343–1350, Oct. 2001.

- [11] N. Pandeya, C. M. Olsen, and D. C. Whiteman, "The incidence and multiplicity rates of keratinocyte cancers in Australia," *Med. J. Aust.*, vol. 207, no. 8, pp. 339–343, Oct. 2017.
- [12] R. L. Wilson, B. A. Yentzer, S. P. Isom, S. R. Feldman, and A. B. Fleischer Jr, "How good are US dermatologists at discriminating skin cancers? A number-needed-to-treat analysis," *J. Dermatological Treat.*, vol. 23, no. 1, pp. 65–69, Feb. 2012.
- [13] J. K. Rivers, M. R. Copley, R. Svoboda, and D. S. Rigel, "Non-invasive gene expression testing to rule out melanoma," *Skin Ther. Lett.*, vol. 23, no. 5, pp. 1–4, Sep. 2018.
- [14] F. Walter, A. Webster, S. Scott, and J. Emery, "The Andersen model of total patient delay: A systematic review of its application in cancer diagnosis," *J. Health Serv. Res. Policy*, vol. 17, no. 2, pp. 110–118, Apr. 2012.
- [15] J. W. Choi et al., "Microwave detection of metastasized breast cancer cells in the lymph node; potential application for sentinel lymphadenectomy," *Breast Cancer Res. Treat.*, vol. 86, no. 2, pp. 107–115, 2004.
- [16] H. Arab, L. Chioukh, M. D. Ardakani, S. Dufour, and S. O. Tatu, "Early-stage detection of melanoma skin cancer using contactless millimeter-wave sensors," *IEEE Sensors J.*, vol. 20, no. 13, pp. 7310–7317, Jul. 2020.
- [17] C. C. Harland, S. G. Kale, P. Jackson, P. S. Mortimer, and J. C. Bamber, "Differentiation of common benign pigmented skin lesions from melanoma by high-resolution ultrasound," *Brit. J. Dermatol.*, vol. 143, no. 2, pp. 281–289, Aug. 2000.
- [18] K. Hoffmann, J. Jung, S. el Gammal, and P. Altmeyer, "Malignant melanoma in 20-MHz B scan sonography," *Dermatology*, vol. 185, no. 1, pp. 49–55, 1992.
- [19] E. Dalimier and D. Salomon, "Full-field optical coherence tomography: A new technology for 3D high-resolution skin imaging," *Dermatology*, vol. 224, no. 1, pp. 84–92, May 2012.
- [20] J. Yun and S.-S. Lee, "Human movement detection and idengification using pyroelectric infrared sensors," *Sensors*, vol. 14, no. 5, pp. 8057–8081, May 2014.
- [21] C. Herman and M. P. Cetingul, "Quantitative visualization and detection of skin cancer using dynamic thermal imaging," *J. Visualized Experiments*, no. 51, 2011, Art. no. e2679.
- [22] P. Aberg, U. Birgersson, P. Elsner, P. Mohr, and S. Ollmar, "Electrical impedance spectroscopy and the diagnostic accuracy for malignant melanoma," *Exp. Dermatol.*, vol. 20, no. 8, pp. 648–652, Aug. 2011.
- [23] P. Aberg, I. Nicander, J. Hansson, P. Geladi, U. Holmgren, and S. Ollmar, "Skin cancer identification using multifrequency electrical impedance— A potential screening tool," *IEEE Trans. Biomed. Eng.*, vol. 51, no. 12, pp. 2097–2102, Dec. 2004.
- [24] D. G. Beetner, S. Kapoor, S. Manjunath, X. Zhou, and W. V. Stoecker, "Differentiation among basal cell carcinoma, benign lesions, and normal skin using electric impedance," *IEEE Trans. Biomed. Eng.*, vol. 50, no. 8, pp. 1020–1025, Aug. 2003.
- [25] M. Lazebnik, E. L. Madsen, G. R. Frank, and S. C. Hagness, "Tissue-mimicking phantom materials for narrowband and ultrawideband microwave applications," *Phys. Med. Biol.*, vol. 50, no. 18, pp. 4245–4258, Sep. 2005.
- [26] D. A. Pollacco, L. Farrugia, M. C. Conti, L. Farina, P. S. Wismayer, and C. V. Sammut, "Characterization of the dielectric properties of biological tissues using mixture equations and correlations to different states of hydration," *Biomed. Phys. Eng. Exp.*, vol. 5, no. 3, Mar. 2019, Art. no. 35022.
- [27] S. Gabriel, R. W. Lau, and C. Gabriel, "The dielectric properties of biological tissues: Ii measurements in the frequency range 10 Hz to 20 GHz," *Phys. Med. Biol.*, vol. 41, no. 11, pp. 2251–2269, Nov. 1996.
- [28] A. Mirbeik-Sabzevari, R. Ashinoff, and N. Tavassolian, "Ultra-wideband millimeter-wave dielectric characteristics of freshly excised normal and malignant human skin tissues," *IEEE Trans. Biomed. Eng.*, vol. 65, no. 6, pp. 1320–1329, Jun. 2018.
- [29] M. Gniadecka, O. F. Nielsen, and H. C. Wulf, "Water content and structure in malignant and benign skin tumours," *J. Mol. Struct.*, vol. 661, pp. 405–410, Dec. 2003.
- [30] H. N. Mayrovitz, S. R. Gildenberg, P. Spagna, L. Killpack, and D. A. Altman, "Characterizing the tissue dielectric constant of skin basal cell cancer lesions," *Skin Res. Technol.*, vol. 24, no. 4, pp. 686–691, Nov. 2018.
- [31] V. Suntzeff and C. Carruthers, "The water content in the epidermis of mice undergoing carcinogenesis by methylcholanthrene," *Cancer Res.*, vol. 6, no. 10, pp. 574–577, Oct. 1946.
- [32] K. G. Stern and R. Willheim, The Biochemistry of Malignant Tumors. Brooklyn, NY, USA: Reference Press, 1943.
- [33] I. L. Mulay, R. Roy, B. E. Knox, N. H. Suhr, and W. E. Delaney, "Trace-metal analysis of cancerous and non-cancerous human tissues," *J. Nat. Cancer Inst.*, vol. 47, no. 1, pp. 1–13, Jul. 1971.

- [34] F. Topfer, S. Dudorov, and J. Oberhammer, "Millimeter-wave near-field probe designed for high-resolution skin cancer diagnosis," *IEEE Trans. Microw. Theory Techn.*, vol. 63, no. 6, pp. 2050–2059, Jun. 2015.
- [35] A. Taeb, S. Gigoyan, and S. Safavi-Naeini, "Millimetre-wave waveguide reflectometers for early detection of skin cancer," *IET Microw., Antennas Propag.*, vol. 7, no. 14, pp. 1182–1186, Nov. 2013.
- [36] P. Mehta, K. Chand, D. Narayanswamy, D. G. Beetner, R. Zoughi, and W. V. Stoecker, "Microwave reflectometry as a novel diagnostic tool for detection of skin cancers," *IEEE Trans. Instrum. Meas.*, vol. 55, no. 4, pp. 1309–1316, Aug. 2006.
- [37] J.-C. Chiao et al., "Applications of microwaves in medicine," *IEEE J. Microw.*, vol. 3, no. 1, pp. 134–169, Jan. 2023.
- [38] S. I. Alekseev, A. A. Radzievsky, M. K. Logani, and M. C. Ziskin, "Millimeter wave dosimetry of human skin," *Bioelectromagnetics*, vol. 29, no. 1, pp. 65–70, Jan. 2008.
- [39] F. Kazemi, F. Mohanna, and J. Ahmadi-shokouh, "Microwave reflectometry for noninvasive imaging of skin abnormalities," *Australas. Phys. Eng. Sci. Med.*, vol. 41, no. 4, pp. 881–890, Dec. 2018.
- [40] F. Kazemi, F. Mohanna, and J. Ahmadi-Shokouh, "Nondestructive high-resolution microwave imaging of biomaterials and biological tissues," AEU - Int. J. Electron. Commun., vol. 84, pp. 177–185, 2018.
- [41] R. Schiavoni, G. Maietta, E. Filieri, A. Masciullo, and A. Cataldo, "Microwave reflectometry sensing system for low-cost in-vivo skin cancer diagnostics," *IEEE Access*, vol. 11, pp. 13918–13928, 2023.
- [42] S. Bing, K. Chawang, and J.-C. Chiao, "A self-tuned method for impedance-matching of planar-loop resonators in conformable wearables," *Electronics*, vol. 11, no. 17, Jan. 2022, Art. no. 2784.
- [43] J. Wei, "Distributed capacitance of planar electrodes in optic and acoustic surface wave devices," *IEEE J. Quantum Electron.*, vol. 13, no. 4, pp. 152–158, Apr. 1977.
- [44] F. Maradei and S. Caniggia, Appendix A: Formulae for Partial Inductance Calculation (Signal Integrity and Radiated Emission of High-Speed Digital Systems Series). Chichester, U.K.: Wiley, Nov. 2008.
- [45] S. Bing, K. Chawang, and J.-C. Chiao, "A resonant coupler for subcutaneous implant," *Sensors*, vol. 21, no. 23, Dec. 2021, Art. no. 8141.
- [46] S. Bing, K. Chawang, and J. C. Chiao, "Resonant coupler designs for subcutaneous implants," in *Proc. IEEE Wireless Power Transfer Conf.*, 2021, pp. 1–4.
- [47] S. Bing, K. Chawang, and J.-C. Chiao, "A flexible tuned radio-frequency planar resonant loop for noninvasive hydration sensing," *IEEE J. Microw.*, vol. 3, no. 1, pp. 181–192, Jan. 2022.
- [48] S. Bing, K. Chawang, and J. C. Chiao, "A radio-frequency planar resonant loop for noninvasive monitoring of water content," in *Proc. IEEE Sensors*, 2022, pp. 1–4.
- [49] S. Bing, K. Chawang, and J.-C. Chiao, "A tuned microwave resonant system for subcutaneous imaging," Sensors, vol. 23, no. 6, 2023, Art. no. 3090.
- [50] T. Takenouchi, "Key points in dermoscopic diagnosis of basal cell carcinoma and seborrheic keratosis in Japanese," *J. Dermatol.*, vol. 38, no. 1, pp. 59–65, Jan. 2011.
- [51] Y. Y. Gao, X. J. An, J. Yang, C. Z. Huang, and J. Tao, "Seborrheic keratosis mimicking basal cell carcinoma under dermoscopy: A case report," *Chin. Med. J.*, vol. 133, no. 17, pp. 2139–2140, Sep. 2020.
- [52] R. Bedir, C. Yurdakul, H. Güçer, and I. Sehitoglu, "Basal cell carcinoma arising within seborrheic keratosis," *J. Clin. Diagn. Res.*, vol. 8, no. 7, Jul. 2014, Art. no. YD06-7.
- [53] S.-Q. Wang et al., "High-frequency ultrasound features of basal cell carcinoma and its association with histological recurrence risk," *Chin. Med. J.*, vol. 132, no. 17, pp. 2021–2026, Sep. 2019.
- [54] C. Longo et al., "Clonal seborrheic keratosis: Dermoscopic and confocal microscopy characterization," *J. Eur. Acad. Dermatol. Venereol.*, vol. 28, no. 10, pp. 1397–1400, Oct. 2014.
- [55] A. Mirbeik-Sabzevari and N. Tavassolian, "Ultrawideband, Stable normal and cancer skin tissue phantoms for millimeter-wave skin cancer imaging," *IEEE Trans. Biomed. Eng.*, vol. 66, no. 1, pp. 176–186, Jan. 2019.
- [56] J. Garrett and E. Fear, "Stable and flexible materials to mimic the dielectric properties of human soft tissues," *IEEE Antennas Wireless Propag. Lett.*, vol. 13, pp. 599–602, 2014.
- [57] "N1501 A dielectric probe kit," Keysight Technol., Santa Rosa, CA, USA, 2020. [Online]. Available: https://www.keysight.com/us/en/assets/7018-04631/technical-overviews/5992-0264.pdf
- [58] D. Andreuccetti, R. Fossi, and C. Petrucci, "An internet resource for the calculation of the dielectric properties of body tissues in the frequency range 10 Hz GHz," 1997. [Online]. Available: http://niremf.ifac.cnr.it/ tissprop/



Sen Bing (Graduate Student Member, IEEE) received the B.Tech. degree in electronics and information science and technology from Hainan Normal University, Haikou, China, in 2017, and the M.S. degree in electrical engineering from Southern Methodist University, Dallas, TX, USA, in 2019. He is currently working toward the Ph.D. degree in electrical and computer engineering with Southern Methodist University. He has authored four journal articles and seven conference papers on optimizing performance for microwave biomedical sensors and implants, co-authored two

journal articles and four conference papers on factors affecting pH performance, and authored one conference paper on low-cost ultrasound medical imaging. His research interests include microwave biomedical devices, electrochemical biosensors, wearable electronics, medical imaging, and RF devices.



Khengdauliu Chawang (Graduate Student Member, IEEE) received the Bachelor of Technology degree in electronics and communication engineering from the National Institute of Technology, India, in 2012, and the Master of Science degree in electrical engineering from the University of Texas at Arlington, Arlington, TX, USA, in 2019. She is currently working toward the Ph.D. degree in the electrical and computer engineering with Southern Methodist University, Dallas, TX, USA. She has authored/co-authored seven conference papers on factors affecting pH performance.

Her research interest include flexible and ultra-flexible devices by micro and nano fabrication, electro-chemical biosensors, wearable electronics, and RF devices.



J.-C. Chiao (Fellow, IEEE) received the B.S. degree from the Electrical Engineering Department, National Taiwan University, Taipei, Taiwan, in 1988, the M.S. and Ph.D. degrees in electrical engineering from the California Institute of Technology, Pasadena, CA, USA, in 1991 and 1995, respectively. He was a Research Scientist of the Optical Networking Systems and Testbeds Group at Bell Communications Research, an Assistant Professor of electrical engineering with the University of Hawaii, Honolulu, HI, USA, and Product Line Manager and Senior Technol-

ogy Advisor with Chorum Technologies. Dr. Chiao was Janet and Mike Greene endowed Professor and Jenkins Garrett Professor of Electrical Engineering with the University of Texas — Arlington, Arlington, TX, USA, from 2002 to 2018. He is currently Mary and Richard Templeton Centennial Chair Professor of electrical and eomputer engineering with Southern Methodist University, Dallas, TX, USA. He has authored or coauthored and edited numerous peer-reviewed technical journal and conference papers, book chapters, proceedings and books. He holds 20 patents in RF MEMS, MEMS optical, liquid crystal, nano-scale fabrication, and wireless medical sensor technologies. His research work covered by media extensively including, Forbes, national geographic magazine, national public radio and CBS henry ford innovation nation. He is the Chair and technical program Chair of several international conferences including 2018 IEEE International Microwave Biomedical Conference (IMBioC) and 2021 IEEE Wireless Power Transfer Conference. He was the Chair for the IEEE MTT-S Technical Committee 10 Biological Effect and Medical Applications of RF and Microwave and an Associate Editor for IEEE TRANSACTIONS ON MICROWAVE THEORY AND TECHNIQUES. He was the founding Editor-in-Chief of theIEEE JOURNAL OF ELECTROMAGNETICS, RF, AND MICROWAVES IN MEDICINE AND BIOLOGY. He is with the Editorial Board of IEEE ACCESS and Track Editor of IEEE JOURNAL OF MICROWAVES. Dr. Chiao was the recipient of Lockheed Martin Aeronautics Company Excellence in Engineering Teaching Award; Tech Titans Technology Innovator Award, Research in Medicine award in the Heroes of Healthcare, IEEE Region 5 Outstanding Engineering Educator award, IEEE Region 5 Excellent Performance award, 2012-2014 IEEE MTT Distinguished Microwave Lecturer, 2017–2019 IEEE Sensors Council Distinguished Lecturer, Pan Wen-Yuan Foundation Excellence in Research Award, and the 2011 Edith and Peter O'Donnell Award in Engineering by The Academy of Medicine, Engineering and Science of Texas. Dr. Chiao is a Fellow of IET, SPIE, and AIMBE.